Materials Transactions, Vol. 47, No. 11 (2006) pp. 2765 to 2772

Phase-Field Simulation of Phase Transformation in Fe-Cu-Mn-Ni Quaternary Alloy

Toshiyuki Koyama[1], Kiyoshi Hashimoto[2] and Hidehiro Onodera[1]

[1]*Computational Materials Science Center, National Institute for Materials Science, Tsukuba 305-0047, Japan*
[2]*Core Research for Evolutional Science and Technology (CREST), Japan Science and Technology, Tsukuba 305-0047, Japan*

The phase decomposition in α(bcc) phase and the subsequent structural phase transformation from α to γ(fcc) phase during isothermal aging of an Fe-Cu-Mn-Ni quaternary alloy, which is a base alloy of the light-water reactor pressure vessel, have been simulated by the phase-field method. At the early stage of spinodal decomposition, Cu-rich α phase is formed, and the Mn and Ni, which are minor components, are partitioned to the Cu-rich phase. As the Cu composition in the precipitate is increased, the Ni atoms inside the precipitates move to the interface region between the precipitate and matrix, but Mn atoms remain inside the Cu particles. When the Cu-rich particles eventually transform to the fcc structure, the Mn atoms also move to the interface region, which results in the shell structure of the fcc Cu precipitates, where each particle is surrounded by a thin layer enriched in Mn and Ni. This microstructural change can be reasonably explained by considering the local equilibrium at the surface region of the Cu-rich particles. [doi:10.2320/matertrans.47.2765]

(Received July 27, 2006; Accepted September 22, 2006; Published November 15, 2006)

Keywords: *phase-field method, segregation, phase separation, phase decomposition, spinodal decomposition, reactor pressure vessel, diffusion equation*

1. Introduction

The phase-field method is effective in understanding the inhomogeneous complex behavior during phase transformations because it has a useful framework that includes the static approach based on the total free energy of microstructures and the dynamic approach to describe the complex microstructure evolutions.[1–9)] In the previous study,[10)] the spinodal decomposition of the α(bcc) phase in an Fe-Cu-Mn-Ni quaternary alloy, which is a base system of the light-water reactor pressure vessel,[11,12)] was simulated by using the phase-field method, and it was pointed out that the segregation of Mn and Ni takes place at the surface of α(bcc) Cu particles. However, the experimental investigation by Osamura *et al.*[13)] concluded that this segregation is not observed at the surface of the α Cu particles but instead at the surface of γ(fcc) Cu particles. Isheim *et al.*[14)] have also recently confirmed the segregation of Mn and Ni at the surface of the γ Cu particles. On the other hand, according to the recent atom-probe tomography investigation by Isheim *et al.*,[15)] segregation takes place also for α Cu particles.

The objective of this study is to extend the previous simulation to calculate not only the diffusion-controlled phase decomposition but also the structural phase transformation from bcc to fcc in the same Fe-Cu-Mn-Ni quaternary alloy. The segregation behavior of Ni and Mn at the surface of the Cu-rich phase, which may depend on its crystal structure, is discussed on the basis of the results of simulation.

2. Calculation Method

Since we focus on the microstructure changes during the diffusion-controlled phase decomposition and the structural phase transformation from bcc to fcc in the Fe-Cu-Mn-Ni quaternary alloy, the independent variables to describe the microstructure changes are the composition fields and the crystal structure field. Therefore, the conventional phase-field method[1)] is used in this work. The details of the non-linear evolution equations and the evaluation of the total free energy of the microstructures are explained in the following sections.

2.1 Evolution equations

The evolution equations governing the phase transformation in the Fe-Cu-Mn-Ni quaternary alloy are written as

$$\begin{aligned}\frac{\partial c_i(\mathbf{r},t)}{\partial t} &= M_i\{s(\mathbf{r},t),T\}\nabla^2\frac{\delta G_{\mathrm{sys}}}{\delta c_i(\mathbf{r},t)}, \quad (i=2,3,4)\\ \frac{\partial s(\mathbf{r},t)}{\partial t} &= -M_s(T)\frac{\delta G_{\mathrm{sys}}}{\delta s(\mathbf{r},t)},\end{aligned} \tag{1}$$

where the local composition field of component i, $c_i(\mathbf{r},t)$, is a function of the spatial position $\mathbf{r}$ and time t. The subscripts $i=1$, 2, 3, and 4 correspond to Fe, Cu, Mn, and Ni, respectively. The phase field variable $s(\mathbf{r},t)$ is the probability of finding an fcc phase at position $\mathbf{r}$ and time t, so that $0\le s(\mathbf{r},t)\le 1$; $s=0$ and $s=1$ correspond to the α(bcc) phase and γ(fcc) phase, respectively. G_{sys} is the total free energy of a microstructure, which is expressed as a function of c_i and s. M_i is the mobility of an atom by diffusion defined by

$$M_i(s,T)\equiv c_{0i}(1-c_{0i})\left\{(1-s)\frac{D_i^{\alpha}(T)}{RT}+s\frac{D_i^{\gamma}(T)}{RT}\right\}, \tag{2}$$

where R is the gas constant, T is temperature, and c_{0i} is the average composition of component i. $D_i^{\varphi}(T)$ is the diffusion constant of component i in phase $\varphi(=\alpha,\gamma)$, where the composition dependence of D_i^{φ} is ignored for simplicity. $M_s(T)$ is the kinetic relaxation coefficient for the development of phase field $s(\mathbf{r},t)$. Since we focus on isothermal phase transformation in this study, *i.e.*, the aging temperature T is constant, the parameters $M_s(T)$ and $D_i^{\varphi}(T)$ are also constant.

2.2 Evaluation of the total free energy of a microstructure

The total free energy, G_{sys}, of a microstructure including the α and γ phases in an Fe-Cu-Mn-Ni alloy is expressed as

$$G_{\mathrm{sys}} = \int_{\mathbf{r}} \left\{ \begin{array}{l} \{1-h(s)\}\{G_c^{\alpha}(c_i,T) + YV_{\mathrm{m}}\varepsilon_0^2(c_i)\} \\ \quad +h(s)G_c^{\gamma}(c_i,T) + Wg^2(s) \\ \quad +\displaystyle\sum_{i=1}^{4}\frac{1}{2}\kappa_c(\nabla c_i)^2 + \frac{1}{2}\kappa_s(\nabla s)^2 \end{array} \right\} d\mathbf{r}, \quad (3)$$

where $G_c^{\alpha}(c_i,T)$ and $G_c^{\gamma}(c_i,T)$ denote the Gibbs energies of the α and γ phases,[16–20] respectively, which are expressed as functions of the composition c_i and temperature T. The numerical parameters required for calculating the Gibbs energies are obtained from the thermodynamic database of equilibrium phase diagrams. Therefore, the present simulation is directly related to the phase diagram of the real alloy system. The Gibbs energy function and the numerical parameters used in this simulation are explained in Appendix. The functions $h(s)$ and $g(s)$ in eq. (3) are defined as $h(s) \equiv s^2(3-2s)$ and $g(s) \equiv s(1-s)$, respectively.[1–6] The third term in the integrand of eq. (3) is the energy barrier for the structural transformation between bcc and fcc phases, and W is a positive constant. The fourth and fifth terms are the gradient energies of the composition and the phase fields, respectively. The coefficients κ_c and κ_s are the gradient energy coefficients, which are assumed to be constant in this study. The quantity $YV_{\mathrm{m}}\varepsilon_0^2(c_i)$ in the first term is the elastic strain energy[21,22] induced from the coherent phase separation in the α phase, where Y is the energy function expressed using elastic constants, and V_{m} is the molar volume. $\varepsilon_0(c_i)$ is the eigen-strain,[23] which is defined as a function of composition as $\varepsilon_0(c_i) = \sum_{i=2}^{4}\eta_i(c_i - c_{0i})$, where η_i is the lattice mismatch[22] of component i calculated by $\eta_i = (a_i - a_1)/a_1$. Parameters a_i and c_{0i} are the lattice constants and the average composition of component i, respectively.

In order to solve eq. (1) numerically, a conventional difference method is employed. Simulations in this paper are performed in one or two dimensions, and the minimum mesh size, b, used in the difference method is defined by $b \equiv L/N$, where N is the number of divisions along the x-direction (or y-direction) and L is the width of the simulation area.

Table 1 Numerical values used for the calculation.

Aging temperature, T/K	873
Gradient energy coefficients /J·m^2·mol^{-1}	$\kappa_c = 5.0\times10^{-15}$, $\kappa_s = 1.0\times10^{-15}$
Parameter, W/J·mol^{-1}	5.0×10^{3}
Molar volume,[25] V_{m}/m^3·mol^{-1}	7.09×10^{-6}
Calculation area, $L\times L$/nm^2	30×30
Total mesh number for difference method, $N\times N$	128×128
Energy function of elastic stiffness,[25] Y/Pa	2.14×10^{11}
Lattice mismatch,[24] η_i, $(i=2,3,4)$	$\eta_2 = 3.29\times10^{-2}$, $\eta_3 = 5.22\times10^{-4}$, $\eta_4 = 4.75\times10^{-4}$
Diffusion coefficients,[25] $D_i^{\varphi}(T) = {}^0D_i^{\varphi}\exp(-Q_i^{\varphi}/RT)$: ${}^0D_i^{\varphi}$/m^2·s^{-1}, Q_i^{φ}/J·mol^{-1}, $(i=2,3,4,\ \varphi=\alpha,\gamma)$	${}^0D_2^{\alpha} = 4.7\times10^{-5}$, $Q_2^{\alpha} = 2.44\times10^{5}$ ${}^0D_2^{\gamma} = 4.3\times10^{-5}$, $Q_2^{\gamma} = 2.80\times10^{5}$ ${}^0D_3^{\alpha} = 1.49\times10^{-4}$, $Q_3^{\alpha} = 2.33\times10^{5}$ ${}^0D_3^{\gamma} = 1.78\times10^{-5}$, $Q_3^{\gamma} = 2.64\times10^{5}$ ${}^0D_4^{\alpha} = 1.4\times10^{-4}$, $Q_4^{\alpha} = 2.46\times10^{5}$ ${}^0D_4^{\gamma} = 1.08\times10^{-5}$, $Q_4^{\gamma} = 2.73\times10^{5}$

The distance and the time are normalized to b and $b^2/D_2^{\alpha}(T)$, respectively, and the quantities having the dimension of energy are normalized to RT. The numerical values of the parameters are summarized in Table 1.

2.3 Calculation conditions

Figures 1(a) and 1(b) show the metastable phase diagrams calculated at 873 K considering the α(bcc) and γ(fcc) phases in the Fe-Cu-Ni and Fe-Cu-Mn ternary alloys, respectively. It is noted that the $(\alpha+\gamma_2)$ two-phase region in the Fe-Cu binary phase diagram is connected with the $(\alpha+\gamma_1+\gamma_2)$ three-phase region with increasing Ni or Mn content, and the $(\gamma_1+\gamma_2)$ two-phase region is largely extended in the ternary system. The average composition of the alloy chosen for the simulation is denoted by the solid circle in the $(\alpha+\gamma_2)$ two-phase region.

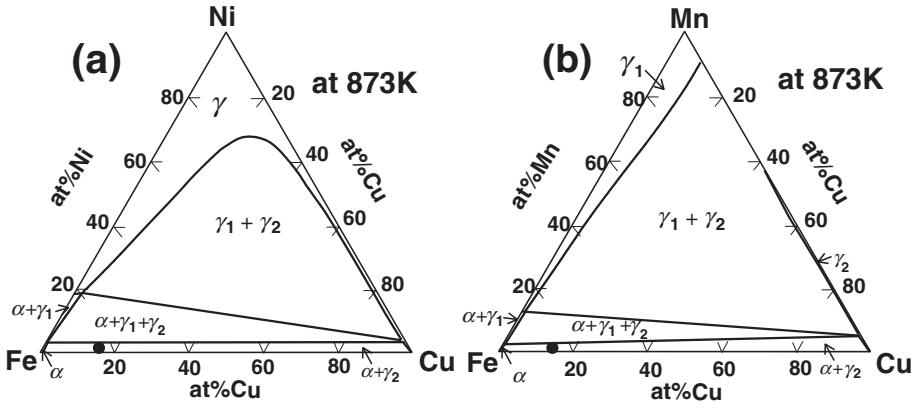

Fig. 1 Calculated metastable phase diagrams of Fe-Cu-Ni and Fe-Cu-Mn ternary alloys where the α(bcc) and the γ(fcc) phases are considered. The average composition of the alloy used for the simulation is denoted by the solid circle in the $(\alpha+\gamma_2)$ two-phase region.

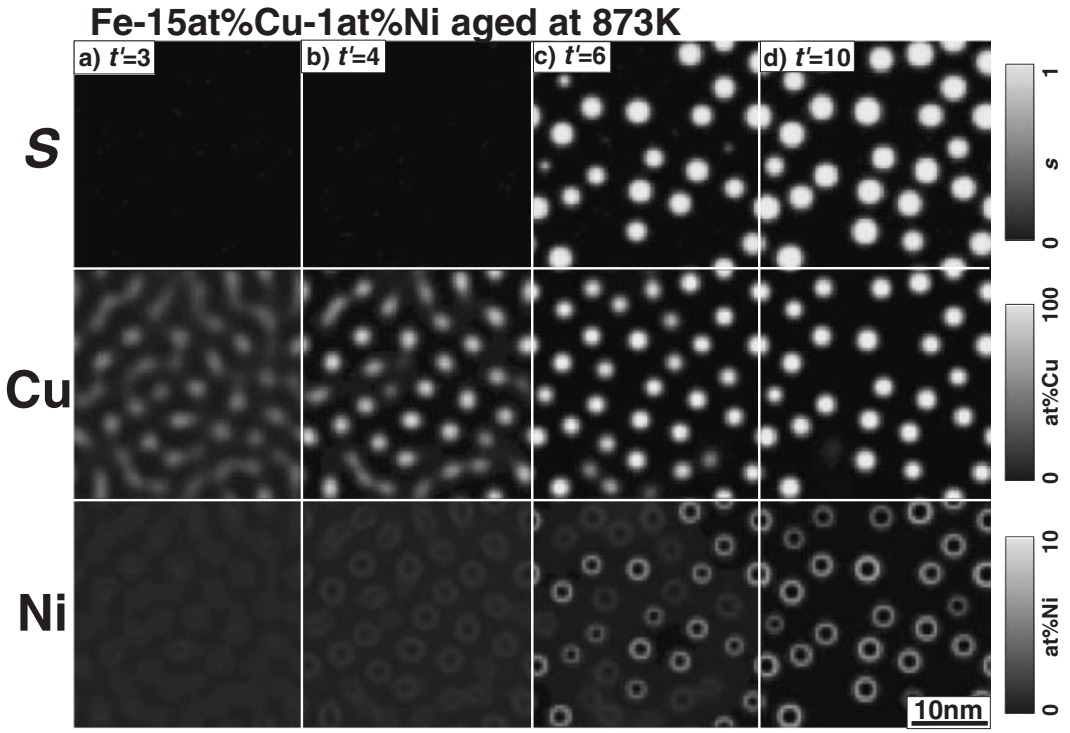

Fig. 2 Two-dimensional simulation of the isothermal phase transformation of the supersaturated solid solution of α phase in an Fe-15 at%Cu-1 at%Ni ternary alloy at 873 K. The top row indicates the phase-field s. The middle and bottom rows are Cu and Ni composition fields, respectively. The numerical values in the figure are normalized time.

3. Simulation Results

3.1 Two-dimensional simulation of an isothermal phase transformation

Figure 2 shows the two-dimensional simulation of the isothermal phase transformation of the supersaturated solid solution of α phase in an Fe-15 at%Cu-1 at%Ni ternary alloy at 873 K. The top row in Fig. 2 indicates the phase-field s. The local value of s is represented by the gray scale, and the brightness is proportional to s. The middle and bottom rows show Cu and Ni composition fields, respectively. The local composition is also indicated by the gray scale, where pure Cu and the 10 at%Ni appear as white (refer to the gray scale marker on the right hand side of Fig. 2). The time scale in Fig. 2 is normalized as explained earlier, *i.e.* the dimensionless time, t', is defined by $t' = t/[b^2/D_2^{\alpha}(T)]$. As for the initial conditions of the supersaturated solid solution of α phase, a small composition fluctuation, followed by random noise using a random number generated by the computer, was imposed.

Figure 2(a) shows the early stage of decomposition of the α phase. The Cu-rich zones are formed homogeneously from the supersaturated solid solution, and Ni atoms are mainly partitioned in the Cu-rich phase. As the Cu composition in the precipitate is increased (Fig. 2(b)), the Ni atoms inside the precipitate move to the interface region between the Cu-precipitate and the matrix. The segregation of Ni at the interface then takes place. Up to this stage, the crystal structure is entirely bcc: the phase field s is zero (completely black) everywhere. The sequence in the microstructure development is the same as that in the previous simulation.[10] With aging, the Cu-rich α phase eventually transforms to the γ phase as indicated by the white particles in the top figure of Fig. 2(c). Simultaneously, the segregation of Ni atoms at the surface of the Cu particle is enhanced, and the location of the segregation shifts toward the center of the Cu particle, *i.e.*, the Ni-rich region of the surface of the Cu particle also assumes the fcc structure. Finally, the shell structure, in which the γ Cu precipitates are surrounded by a thin layer with a high concentration of the Ni component, appears (Fig. 2(d)).

Figure 3 shows the simulation of the isothermal phase transformation in an Fe-15 at%Cu-1 at%Mn ternary alloy at 873 K. The presentation is the same as in Fig. 2, except that the bottom row represents the Mn composition field. In the early stage of aging, Cu-rich zones are formed, and Mn is mainly partitioned in the Cu-rich phase. As the Cu concentration inside the precipitate is increased, the Mn concentration also increases inside the Cu particles, but Mn segregation does not occur, which is different from the result of the previous simulation.[10] As aging progresses, the Cu-rich α phase transforms to the γ phase (Fig. 3(c)). The segregation of Mn atoms at the surface of the Cu particle takes place, and the Mn-rich region of the surface of the Cu particle assumes the fcc structure. Finally, the shell structure similar to that in Fig. 2(d) appears (Fig. 3(d)).

Figure 4 shows the simulation of the isothermal phase transformation in an Fe-15 at%Cu-1 at%Mn-1 at%Ni quaternary alloy at 873 K. The lower two rows show Ni and Mn composition fields. The simulated microstructural evolution looks almost like a combination of Fig. 2 and Fig. 3. In the early stage, Cu-rich zones appear, and Ni and Mn atoms are

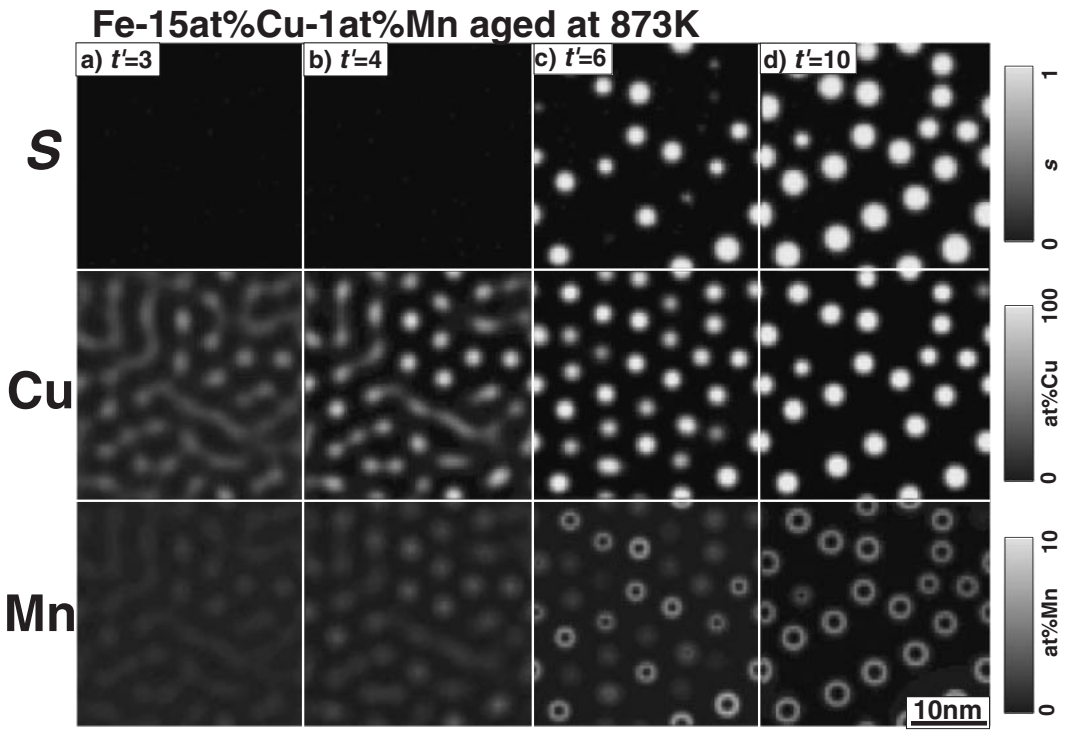

Fig. 3 Two-dimensional simulation of the isothermal phase transformation of the supersaturated solid solution of α phase in an Fe-15 at%Cu-1 at%Mn ternary alloy at 873 K. The presentation is the same as in Fig. 2.

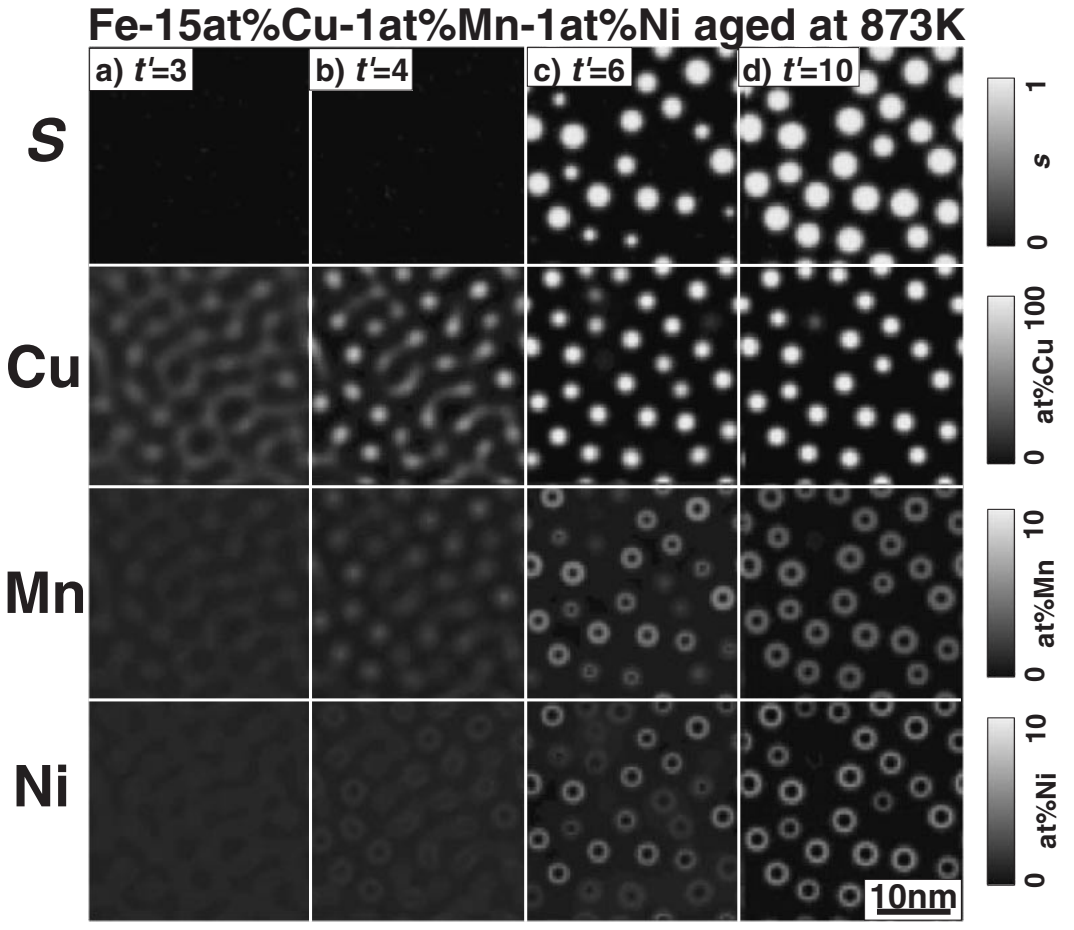

Fig. 4 Two-dimensional simulation of the isothermal phase transformation of the supersaturated solid solution of α phase in an Fe-15 at%Cu-1 at%Mn-1 at%Ni ternary alloy at 873 K.

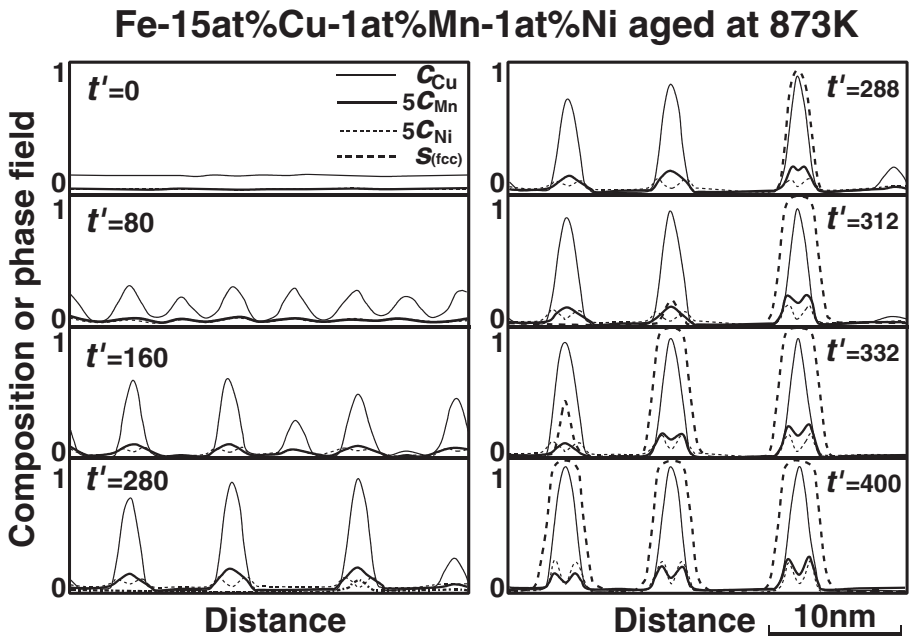

Fig. 5 One-dimensional simulation of the temporal development of the composition and phase-field profiles in an Fe-15 at%Cu-1 at%Mn-1 at%Ni alloy at 873 K. The ordinate represents the solute compositions or the phase-field, *s*, and the abscissa is distance. The thin, thick, and dotted curves correspond to the Cu, Mn, and Ni composition profiles, respectively, and the Mn and Ni compositions are magnified 5 times. The thick dotted curve indicates the phase-field *s*.

partitioned in the Cu-rich phase (Fig. 4(a)). As aging progresses, the Ni atoms inside the precipitates move to the interface region between the precipitate and matrix. Mn atoms do not move to the surface of the Cu particle, and the Mn concentration in the center of the Cu particle is increased. In the later stage of aging, the Cu-rich α phase eventually transforms to the γ phase (Fig. 4(c)), and the segregation of Ni atoms at the surface of the Cu particle is enhanced. Segregation of Mn atoms also takes place, and then the shell structure appears (Fig. 4(d)).

3.2 Temporal changes in the solute composition profile and phase-field during phase transformation in the Fe-Cu-Mn-Ni alloy

Figure 5 shows a one-dimensional simulation of the temporal evolution of the composition and phase-field profiles in an Fe-15 at%Cu-1 at%Mn-1 at%Ni alloy at 873 K. The ordinate represents the solute compositions or the phase-field, *s*, and the abscissa is distance. The thin, thick, and dotted curves correspond to the Cu, Mn, and Ni composition profiles, respectively. The Mn and Ni compositions are magnified 5 times so as to see the segregation behavior easily. The thick dotted curve shows the phase-field *s*.

In the early stage, Cu-rich zones are formed from the supersaturated solid solution, and the Ni and Mn atoms are partitioned in the Cu-rich phase (see the profile at $t' = 80$, in which the profiles of Mn and Ni almost overlap). As aging progresses, the Ni atoms inside the precipitates move to the interface region between the precipitate and matrix. Mn atoms do not move to the surface of the Cu particle. However, the Mn concentration at the center of the Cu particle is increased (see the profile at $t' = 280$). When the Cu-rich α phase transforms to the γ phase, the segregation of Ni atoms at the surface of the Cu particle is enhanced. Segregation of Mn also takes place (see the profile from $t' = 288$ to $t' = 400$).

Looking at the final profile at $t' = 400$, the composition peaks for Cu, Mn, and Ni are found to be located mainly inside the peak of the phase field *s*, which means that the solute-rich region, *i.e.* Cu, Mn, and Ni rich regions, have the fcc structure. This is understood reasonably well considering that Cu has the fcc structure in the standard state and Mn and Ni are the fcc-stabilizing elements for Fe.

4. Discussion

In this section, the segregation behavior of Ni and Mn atoms at the surface of the Cu-rich phase is discussed along the lines of the idea proposed in the previous study.[10] From the composition profiles in Fig. 5, we can obtain the local composition at any point in the microstructure. The local composition taken from Fig. 5 are plotted on the phase diagram in Fig. 6 (the dotted and thick solid curves). These curves correspond to the composition profile of the two-phase mixture $(\alpha_1 + \alpha_2)$ at $t' = 280$ and that of $(\alpha + \gamma_2)$ at $t' = 400$. The solid circle in Fig. 6 indicates the alloy composition. In the early stage of phase decomposition at $t' = 280$, the trajectory of the Ni composition profile on the phase diagram deviates slightly from the tie-line (see the dotted curve of Fig. 6(a)), whereas that of Mn in Fig. 6(b) lies closely to the tie-line direction. (The tie-line is almost parallel to the bottom line of the $(\alpha + \gamma_1 + \gamma_2)$ three-phase region in the phase diagram; see Fig. 1.) However, in the later stage, at $t' = 400$, the trajectory of the Ni and Mn composition profiles on the phase diagram deviates greatly from the tie-line (see

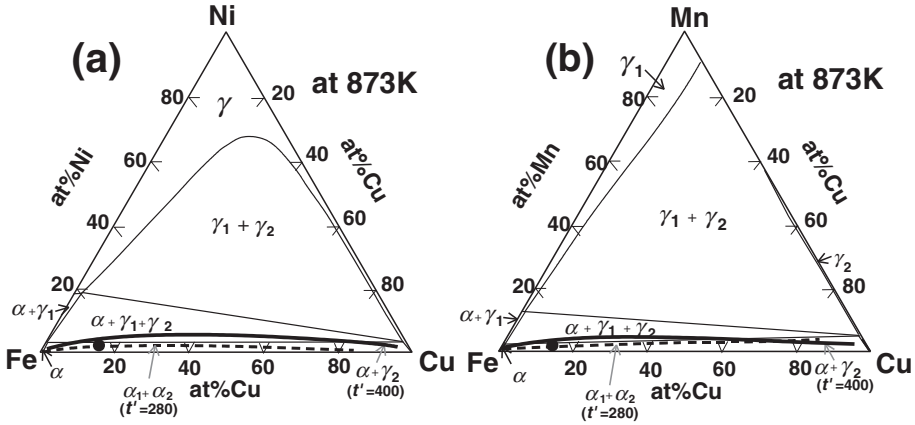

Fig. 6 The trajectories of the composition profiles on the phase diagrams. The dotted curve and the thick solid one at the lower side of each phase diagram are the trajectories corresponding to the composition profiles at $t' = 280$ and $t' = 400$ of Fig. 5, respectively. The solid circle indicates the alloy composition.

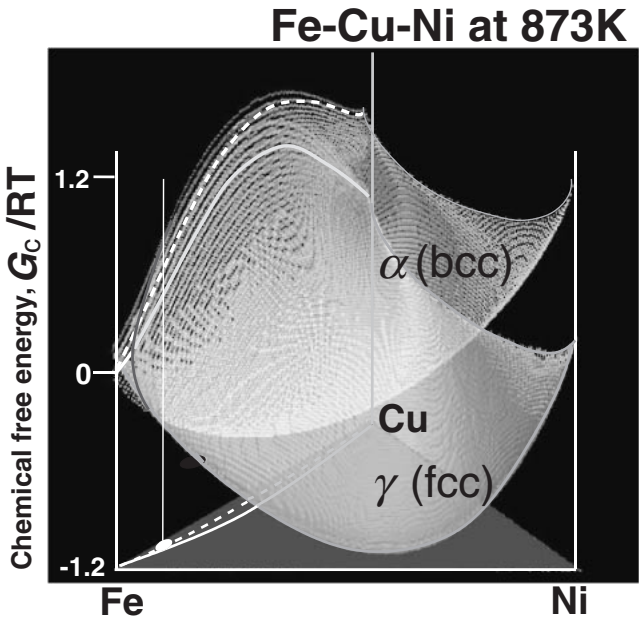

Fig. 7 The Gibbs energy surface of the Fe-Cu-Ni ternary system at 873 K calculated by using the thermodynamic parameters of the phase diagram of the Fe-Cu-Ni alloy, where the upper energy surface is for the α(bcc) phase and the lower one is for the γ phase. The dotted and solid curves on the bottom plane correspond to the dotted and thick solid curves of Fig. 6(a), respectively, and the solid circle on the bottom plane indicates the alloy composition. The dotted and solid curves on the free energy surface plot the trajectories along the curves on the bottom plane.

the thick solid curves in Fig. 6), which indicates that Ni and Mn atoms segregated at the interface region, *i.e.* the compositions of Ni and Mn are high at the surface region of Cu particles, where the Cu composition is about 50%.

The reason why this segregation phenomenon takes place is reasonably explained by considering the local equilibrium at the compositionally diffused interface region of Cu-rich nano-particles. Figure 7 shows the Gibbs energy surface of the Fe-Cu-Ni ternary system at 873 K calculated by using the thermodynamic parameters of the phase diagram of the Fe-Cu-Ni system (see Appendix), where the upper energy surface is for the α phase and the lower one is for the γ phase. When we look at the global shape of the Gibbs energy surface, there is a convex part on the Fe-Cu side, which produces a large driving force for the phase separation between the Cu-rich phase and the Fe-rich phase. This driving force for phase separation decreases rapidly with increasing the Ni content. Comparing this energy reduction with the increase in the Ni content between the α and γ phases, we note that the energy decrease is larger for the case of the γ phase compared with the α phase. That is, the Gibbs energy surface of the γ phase has a steeper slope along the direction to the Ni-rich corner.

The dotted and solid curves on the bottom plane of Fig. 7 correspond to the dotted and thick solid curves of Fig. 6(a), respectively, and the solid circle on the bottom plane in Fig. 7 indicates the alloy composition. The dotted and solid curves on the free energy surface plot the trajectories along the curves on the bottom plane. If the trajectory curve expands towards the Ni-rich corner, the local chemical free energy in the surface region of the Cu-rich particle is decreased, as discussed in the previous study.[10] (That is represented in Fig. 7 of Reference 6.) The reason for this segregation is a local equilibrium of the chemical free energy at the interface region.

In particular, the amount of energy reduction due to this segregation strongly depends on the shape of the free energy surface. When we compare the Gibbs energy surface of the α phase to that of the γ phase in Fig. 7, the energy reduction due to the segregation is larger for the case of the γ phase. Therefore, the segregation tendency should be stronger for the γ phase. This is an essential reason for the enhancement of segregation with the structural transformation from α to γ in Cu particles.

In the previous simulation,[10] Mn segregated during the phase decomposition in the α phase. This was not observed in the present simulation. This is because the concentration of Mn in this study, *i.e.* 1 at%Mn, is lower than that in the previous simulation, 5 at%. However, Mn segregation takes place in the γ phase even at the low concentration in this work because of the steeper slope of the Gibbs energy surface of the γ phase (see Fig. 7). In summary, whether segregation of the solute atoms occurs or not depends on the alloy

composition and aging temperature. The segregation takes place in both the Cu-rich α and γ phases under appropriate conditions. However, the segregation at the surface of the γ phase is more pronounced and thus easily detectable in experiment than the case of the α phase.

5. Conclusions

Isothermal phase transformation in an Fe-Cu-Mn-Ni alloy was simulated on the basis of the phase-field method, and the segregation behavior of Mn and Ni atoms was analyzed. The results obtained are as follows:

(1) At the early stage of spinodal decomposition, Cu-rich α phase is formed, and Mn and Ni atoms are partitioned to the Cu-rich phase. As the Cu composition in the precipitate is increased, the Ni atoms inside the precipitates move to the interface region between the precipitate and matrix. Mn atoms do not move to the surface of the Cu particles, and the Mn concentration at the center of the Cu particles is increased. When the Cu-rich α phase eventually transforms to the γ phase, the segregation of Ni atoms at the surface of the Cu particles is enhanced, and Mn segregation also takes place. Finally, shell structure appears in which the Cu precipitates are surrounded by a thin layer enriched in Mn and Ni.
(2) Whether the segregation of Mn and Ni occurs or not depends on the alloy composition and aging temperature.
(3) Segregation takes place in both the α and γ phases under appropriate conditions, but the segregation at the surface of the γ phase is more pronounced and thus easily detectable in experiment than the case of the α phase.

Acknowledgements

This work was partly supported by a NEDO International Joint Research Grant from the "Nanometal Technology Project" from the Ministry of Education, Culture, Sport, Science, and Technology. This work was supported also by the NAREGI Nanoscience Project, Ministry of Education, Culture, Sports, Science, and Technology, and the CREST, Japan Science and Technology Agency.

REFERENCES

1) T. Koyama: Materia Japan **42** (2003) 397.
2) T. Koyama: Ferrum **9** (2004) 240.
3) T. Koyama: Ferrum **9** (2004) 301.
4) T. Koyama: Ferrum **9** (2004) 376.
5) T. Koyama: Ferrum **9** (2004) 497.
6) T. Koyama: Ferrum **9** (2004) 905.
7) L.-Q. Chen: Ann. Rev. Mater. Res. **32** (2002) 113.
8) W. J. Boettinger, J. A. Warren, C. Beckermann and A. Karma: Ann. Rev. Mater. Res. **32** (2002) 163.
9) M. Ode, S. G. Kim and T. Suzuki: ISIJ Int. **41** (2001) 1076.
10) T. Koyama and H. Onodera: Mater. Trans. **46** (2005) 1187.
11) Kinzoku(Materials Science & Technology), Agne gijutsu center **73** (2003) 721–778.
12) Y. Nagai, T. Toyama, Z. Tang, M. Hasegawa, S. Yanagita, T. Ohkubo and K. Hono: Mater. Sci. Forum **445–446** (2004) 11.
13) K. Osamura, H. Okuda, K. Asano, M. Furusaka, K. Kishida, F. Kurosawa and R. Uemori: ISIJ Inter. **34** (1994) 346–354.
14) D. Isheim, R. P. Kolli, M. E. Finea and D. N. Seidman: Scripta Mater. **55** (2006) 35.
15) D. Isheim, M. S. Gagliano, M. E. Fine and D. N. Seidman: Acta Mater. **54** (2006) 841.
16) N. Saunders and A. P. Miodownik: "*CALPHAD*", Pergamon Materials Series vol. 1, R. W. Cahn ed., (Elsevier Science, Oxford, 1998).
17) A. T. Dinsdale: CALPHAD **15** (1991) 317.
18) J. Miettinen: Computer Coupling of Phase Diagrams and Thermochemistry **27** (2003) 141.
19) SSOL database in "ThermoCalc (ver.M)", Thermo-Calc Software AB.
20) M. Hillert and M. Jarl: CALPHAD **2** (1978) 227.
21) J. W. Cahn and J. E. Hilliard: J. Chem. Phys. **28** (1958) 258.
22) J. E. Hilliard: *Phase Transformation*, ed. by H. I. Aaronson, (ASM, Metals Park, Ohio, 1970) pp. 497–560.
23) T. Mura: *Micromechanics of Defects in Solids*, 2nd Rev. Ed., (Kluwer Academic Publishers, Dordrecht, Netherlands, 1991).
24) W. B. Pearson ed.: *A Handbook of Lattice Spacings and Structures of Metals and Alloys*, (Pergamon, New York, 1967).
25) *Metals data book*, 3rd Ed., Japan Institute of Metals ed., Maruzen, Tokyo, Japan, 1993.

Appendix: (Gibbs energy function used for the simulation)

The Gibbs energy function of phase φ phase ($\varphi = \alpha$ or γ) in an Fe-Cu-Mn-Ni quaternary system with a magnetic contribution is described by the sub-regular solution approximation,[16]

$$G_c^{\varphi}(c_i, T) = \sum_i G_i^{\varphi} c_i + {}^{\mathrm{E}}G^{\varphi} + {}^{\mathrm{mg}}G^{\varphi} + RT \sum_i c_i \ln c_i, \qquad (\mathrm{A}\cdot 1)$$

where G_i^{φ} is the Gibbs energy of the φ phase of pure element i, which is expressed as a function of temperature.[17] ${}^{\mathrm{E}}G^{\varphi}$ is the excess energy corresponding to the heat of mixing, and ${}^{\mathrm{mg}}G^{\varphi}$ is the magnetic contribution to the Gibbs energy. The functions ${}^{\mathrm{E}}G^{\varphi}$ and ${}^{\mathrm{mg}}G^{\varphi}$ are defined as

$${}^{\mathrm{E}}G^{\varphi} \equiv \sum_i \sum_{j>i} L_{i,j}^{\varphi} c_i c_j + \sum_i \sum_{j>i} \sum_{k>j} L_{i,j,k}^{\varphi} c_i c_j c_k, \qquad (\mathrm{A}\cdot 2)$$

$${}^{\mathrm{mg}}G^{\varphi} \equiv RT \ln(\beta^{\varphi} + 1) f(\tau), \quad \tau \equiv T/T_{\mathrm{C}}^{\varphi}, \qquad (\mathrm{A}\cdot 3)$$

where the interaction parameters $L_{i,j}^{\varphi}$ and $L_{i,j,k}^{\varphi}$, the Curie temperature T_{C}^{φ}, and the atomic magnetic moment β^{φ} are available from the thermodynamic database of equilibrium phase diagrams. The parameters for the Fe-Cu-Mn alloy have been determined by Miettinen,[18] and the parameters for the Fe-Cu-Ni alloy are available from the SSOL database in the software package ThermoCalc.[19] We used the following data:

$${}^{0}G_1^{\alpha} = 0, \quad {}^{0}G_2^{\alpha} = 4017 - 1.255T,$$
$${}^{0}G_3^{\alpha} = -3235.3 + 127.85T - 23.7T \ln T - 0.00744271T^2 + 60000/T,$$
$${}^{0}G_4^{\alpha} = 8715.084 - 3.556T,$$

$$
\begin{aligned}
&{}^0G_1^\gamma = -1462.4 + 8.282T - 1.15T\ln T + 6.4\times 10^{-4}T^2, \quad {}^0G_2^\gamma = 0,\\
&{}^0G_3^\gamma = -3439.3 + 131.884T - 24.5177T\ln T - 0.006T^2 + 69600/T, \quad {}^0G_4^\gamma = 0,\\
&L_{1,2}^\alpha = 41033.0 - 6.022T,\\
&(L_{1,2}^\alpha = 39257.976 - 4.1498304T : \text{used only for the simulation of Fe-Cu-Ni}),\\
&L_{1,3}^\alpha = -2759.0 + 1.237T, \quad L_{1,4}^\alpha = -956.63 - 1.28726T + (1789.03 - 1.92912T)(c_1 - c_4),\\
&L_{2,3}^\alpha = 11190.0 - 6.0T - 9865.0(c_2 - c_3), \quad L_{2,4}^\alpha = 8366.0 + 2.802T,\\
&L_{3,4}^\alpha = -51638.31 + 3.64T + 6276.0(c_3 - c_4),\\
&L_{1,2,3}^\alpha = 30000.0, \quad L_{1,2,4}^\alpha = L_{1,3,4}^\alpha = L_{2,3,4}^\alpha = 0,\\
&L_{1,2}^\gamma = (53360 - 12.626T) + (11512 - 7.095T)(c_2 - c_1),\\
&(L_{1,2}^\gamma = (48232.565 - 8.6095425T) + (8861.8816 - 5.2897513T)(c_2 - c_1) :\\
&\quad \text{used only for the simulation of Fe-Cu-Ni})\\
&L_{1,3}^\gamma = (-7762 + 3.865T) + (-259)(c_1 - c_3),\\
&L_{1,4}^\gamma = (-12054.355 + 3.27413T) + (11082.1315 - 4.45077T)(c_1 - c_4) + (-725.805174)(c_1 - c_4)^2,\\
&L_{2,3}^\gamma = (11820 - 2.3T) + (-10600 + 3T)(c_2 - c_3) + (0)(c_2 - c_3)^2 + (-4850 + 3.5T)(c_2 - c_3)^3,\\
&L_{2,4}^\gamma = (8366 + 2.802T) + (-4359.6 + 1.812T)(c_2 - c_4), \quad L_{3,4}^\gamma = (-58158 + 10.878T) + (6276)(c_3 - c_4),\\
&L_{1,2,3}^\gamma = -68000 + 50T, \quad L_{1,2,4}^\gamma = -73272 + 30.9T, \quad (\text{J/mol})\\
&T_C^\alpha = 1043c_1 - 580c_3 + 575c_4 + 123c_1c_3,\\
&T_C^\gamma = -201c_1 - 1620c_3 + 633c_4 + c_1c_3\{-2282 - 2068(c_1 - c_3)\} + c_1c_4\{2133 - 682(c_1 - c_4)\}\\
&\qquad + c_2c_4\{-935.5 - 594.9(c_2 - c_4)\} + 7000c_1c_2c_4, \quad (\text{K})\\
&\beta^\alpha = 2.22c_1 - 0.27c_3 + 0.85c_4,\\
&\beta^\gamma = -2.1c_1 - 1.86c_3 + 0.52c_4 + 20c_1c_2c_4 + c_2c_4\{-0.7316 - 0.3174(c_2 - c_4)\}\\
&\qquad + c_1c_4\{9.55 + 7.23(c_1 - c_4) + 5.93(c_1 - c_4)^2 + 6.18(c_1 - c_4)^3\}
\end{aligned}
$$

The function $f(\tau)$ in eq. (A·3) is given by Hillert and Jarl[20] as a function of τ, which is a dimensionless temperature normalized to the Curie temperature, given by $\tau = T/T_C^\varphi$, $(\varphi = \alpha, \gamma)$.

$$
\begin{aligned}
&f(\tau) \equiv 1 - \frac{1}{D}\left\{\frac{79\tau^{-1}}{140p} + \frac{474}{497}\left(\frac{1}{p} - 1\right)\left(\frac{\tau^3}{6} + \frac{\tau^9}{135} + \frac{\tau^{15}}{600}\right)\right\}, (\tau \le 1),\\
&f(\tau) \equiv -\frac{1}{D}\left(\frac{\tau^{-5}}{10} + \frac{\tau^{-15}}{315} + \frac{\tau^{-25}}{1500}\right), \quad (\tau > 1),\\
&D \equiv \frac{518}{1125} + \frac{11692}{15975}\left(\frac{1}{p} - 1\right), (p = 0.4 \text{ for the bcc phase, and } p = 0.28 \text{ for all others}).
\end{aligned}
\tag{A·4}
$$

If β^φ or T_C^φ, $(\varphi = \alpha, \gamma)$ is negative, the following conversion is required: $\beta^\varphi \Rightarrow -\beta^\varphi$ and $T_C^\varphi \Rightarrow -T_C^\varphi$ for the α(bcc) phase, and $\beta^\varphi \Rightarrow -\beta^\varphi/3$ and $T_C^\varphi \Rightarrow -T_C^\varphi/3$ for the γ(fcc) phase.